An SIW Quasi-Elliptic Filter with a Controllable Bandwidth Based on Cross Coupling and Dual-Mode Resonance Cavity

Xiang An[*]**, Qi Zhou, and Zhi-Qing Lv**

Abstract—In this paper a substrate integrated waveguide (SIW) quasi-elliptic filter with a controllable bandwidth is proposed. The quasi-elliptic filter response is caused by the cross coupling technique and a dual-mode resonance cavity. The dual-mode resonance cavity with TE_{101} and TE_{102} modes is used to generate the passband, and the cross coupling provides two signal transmission paths to produce transmission zeros (TZs). The bandwidth of the filter can be controlled by a pair of disturbing metallic via-holes. A quasi-elliptic filter with the center frequency of 11.03 GHz is designed, fabricated and measured. The experiment data agree well with the simulated ones.

1. INTRODUCTION

With the rapid development of wireless, mobile, sensing and communication systems, the demand for the selectivity of filters is getting higher and higher. Elliptic or quasi-elliptic filters gain much attention in the industry, since they have finite transmission zeros (TZs) to improve the selectivity of passband. One of the most popular ways to produce finite TZs and obtain an elliptic or quasi-elliptic filtering performance is the cross coupling technique. The substrate integrated waveguide (SIW) has been successfully employed in various filters due to the advantages of high quality factor, low insertion loss, and easy integration with planar circuits [1]. Many elliptic or quasi-elliptic filters are designed using SIW cavities [2–5]. In [3], a series of two-layer SIW elliptic filters with controllable electric and magnetic mixed coupling are proposed. Due to the mixed coupling, controllable TZs can be produced below or above the passband. A Ka-band quadruple filter with coplanar waveguide (CPW) line to implement negative cross-coupling structure is designed and discussed in [5], and with the help of this structure, it will be easy to adjust the position of TZs by changing the length of the CPW line. In addition, a new trend of SIW application is multi-mode filters [6–8], since multi-mode SIW filters have the advantages of sharp shirt selectivity and compact structure. In [6] a novel approach is proposed to design a class of triple-mode bandpass filters on SIW structure; the three modes are generated by complementary split-ring resonator (CSRR) and degenerate modes of an SIW rectangular cavity. This method comes up with an easy way to control the inband resonant point as well as the TZs by adjusting the position of the disturbing via-holes and the dimensions of CSRR.

In this work, an SIW quasi-elliptic filter with a controllable bandwidth is presented. The design scheme is based on the cross coupling technique and a dual-mode resonance cavity. We employ the traditional cascaded triplet (CT) topology to design a filter model as a basic model. Then, we introduce a dual-mode resonance cavity, and we can adjust the resonant point of the cavity. To generate a passband with two TZs at each side of the passband, we put a pair of disturbing metallic via-holes in the dual-mode resonance cavity to compress the electric field in the cavity. The bandwidth of the filter can also be controlled by the via-holes. Besides, the location of TZs of traditional SIW cross coupling filter could be generally adjusted by changing the size of the metallic coupling windows, but in this work we

* Corresponding author: Xiang An (afd@mail.xidian.edu.cn).
The authors are with the School of Electronic Engineering, Xidian University, Xi'an 710071, China.

could adjust the distance of the disturbing metallic via-holes and the diameters of theirs to change the location of TZs and bandwidth, which provides one more dimension to adjust the filter. According to the design scheme, a filter is simulated, fabricated and measured. The measured results and simulation data are in good agreement.

2. DESIGN PROCEDURE

2.1. SIW Filter with CT Topology

An SIW resonance cavity could be regarded as a capacitance-Inductance parallel resonant circuit. When signal transmits through it, the phase shift will be zero at the resonant point, whereas it become $+90°$ and $-90°$ at the lower and upper ends of the resonant frequency, respectively. Generally, the electric coupling between two resonators could be treated as a capacitance, which can cause a $+90°$ phase shift. As a duality, magnetic coupling can be treated as an inductance, and it can cause the phase to shift $-90°$ [9].

Most TZs are realized by setting different signal transmission paths between resonators and make the multi-paths have different phases but the same magnitude at one or more frequency points [10]. Traditional CT topology filters use three resonators to generate two different signal transmission paths, which have a $180°$ phase difference and lead to a TZ at the lower stopband or the upper one. A CT phase model is shown in Fig. 1, in which R_1, R_2, R_3 represent the three resonators, respectively. As shown in Table 1, the path R_1-R_2-R_3 and the path R_1-R_3 have a $180°$ phase difference below the resonance point, which causes a TZ at the lower stopband. In accordance with this, we use three SIW cavities to generate three resonators and design a filter, as shown in Fig. 2.
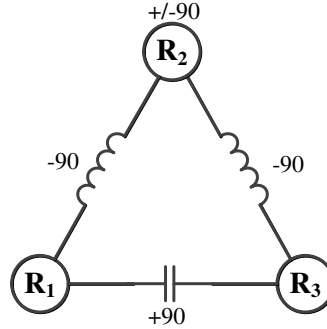

Figure 1. CT phase model.

Table 1. Phase of the CT shown in Fig. 1.

Path	Below resonance	Above resonance
R_1-R_2-R_3	$-90° + 90° - 90° = -90°$	$-90° - 90° - 90° = -270°$
R_1-R_3	$+90°$	$+90°$
Result	out of phase	in phase

The three square SIW cavities are marked as R_1, R_2, and R_3, respectively. The magnetic couplings between R_1 and R_2, and the one between R_2 and R_3 are realized by the metallic coupling windows, as shown in Fig. 2. However, the electric coupling between R_1 and R_3 is achieved by etching a pair of axisymmetric "S" shaped slots [11] on the top layer and the ground layer (not shown in Fig. 2), respectively. There are two transmission paths, namely R_1-R_2-R_3 and R_1-R_3. We use the CPW SIW-microstrip line transition, as shown in Fig. 2, to excite the feed line. The substrate has a dielectric constant of 2.2 and thickness of 0.508 mm. The simulated S-parameter of the filter is plotted in Fig. 3.
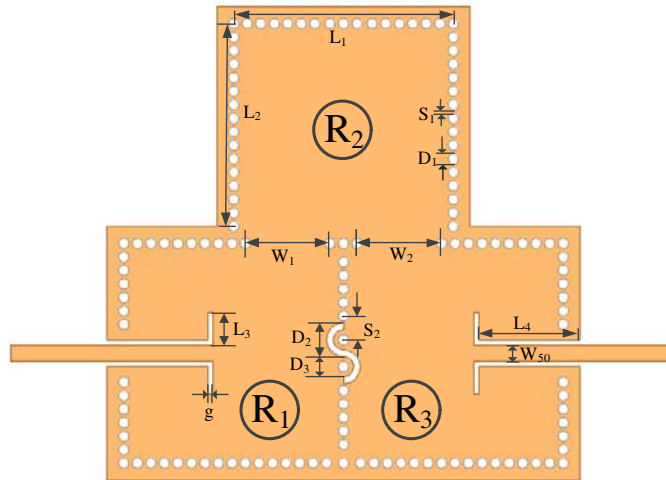
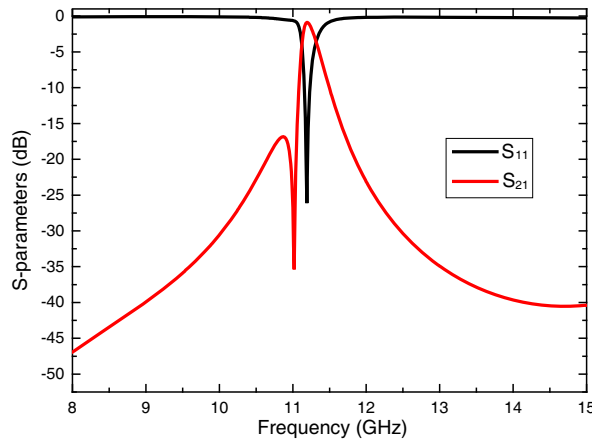**Figure 2.** Top view of the SIW filter with CT topological structure.

Figure 3. Simulated S-parameter of the filter shown in Fig. 2. The dimensions: $W_1 = 5$, $W_2 = 5$, $L_1 = 13$, $L_2 = 13$, $L_3 = 1.92$, $L_4 = 6$, $S_1 = 0.8$, $S_2 = 1.4$, $g = 0.3$, $W_{50} = 1$, $D_1 = 0.3$, $D_2 = 2$, $D_3 = 1.2$ (all in mm).

As can be seen, the resonant point lies at 11.19 GHz, and only one TZ is located below the resonance at 11.02 GHz.

2.2. CT Topology Based SIW Filter with Dual-Mode Resonance Cavity

The SIW cavities discussed in Section 2.1 only use the first-order mode of cavity, namely the TE_{101} mode, to realize the couplings among them. Now, we double the width of the cavity R_2, while other parameters are fixed, as shown in Fig. 4. Thus, it will excite the TE_{102} mode at the same frequency as the one of TE_{101} mode.

Because the resonator R_2 use both the TE_{101} and the TE_{102} modes, while the resonator R_1 and R_3 only have TE_{101} mode, we name R_1 and R_3 as TE_{101} mode resonators, and R_2 as TE_{102} mode resonator, respectively. The magnetic field distribution in the dual-mode cavity is shown in Fig. 5. The couplings on transmission path R_1-R_2-R_3 are illustrated in Fig. 6.

At the right metallic coupling window (see Fig. 4), the magnetic field of TE_{101} mode and that of TE_{102} mode are in opposite directions, which is marked by the red circle in Fig. 5. This will cause a 180° phase shift in the cavity R_2 and change the CT phase model, as shown in Fig. 6. The corresponding
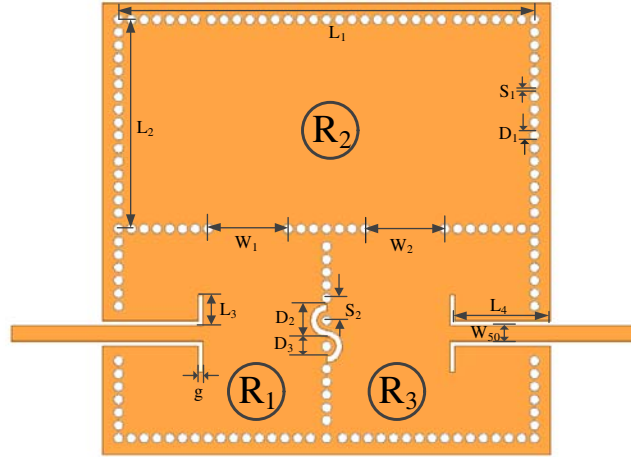
Figure 4. Top view of the CT topology based SIW filter with dual-mode resonance cavity.
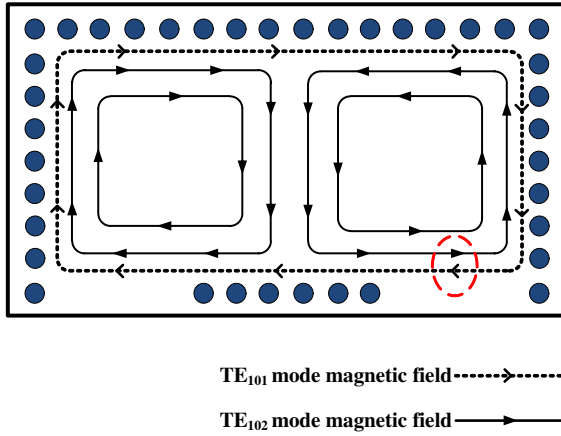

TE$_{101}$ mode magnetic field ------>------

TE$_{102}$ mode magnetic field ———————

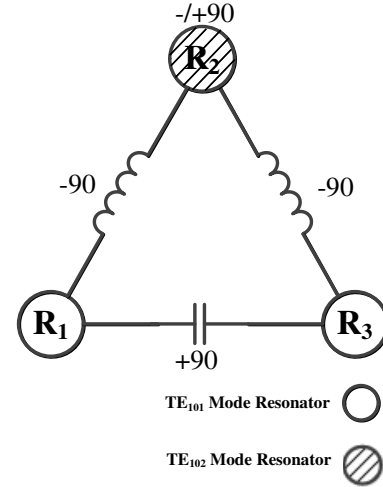**Figure 5.** The magnetic field distribution in dual-mode cavity.

Figure 6. CT phase model in the dual-mode resonance cavity shown in Fig. 4.

analysis of phase is given in Table 2.

From Table 2, we can see that the two transmission paths have a 180° phase difference above resonance, and this will produce a TZ at the upper stopband. This is verified by the simulation data shown in Fig. 7. Comparing Fig. 3 with Fig. 7, we can see that the resonant point is at 11.04 GHz, and the TZ located at 11.32 GHz has shifted from left side of the resonance to the right side. We can also see, from Fig. 7, that there is also a resonant point $f_{\mathrm{TE}_{101}}$ of TE$_{101}$ mode in the cavity R_2, and a transmission zero TZ_1 is located at 8.55 GHz.

2.3. Disturbing Via-Holes

To compress field distribution of TE$_{101}$ mode [12] without affecting the TE$_{102}$ mode, we employ a pair of disturbing metallic via-holes, which are located at the place where the strength of the electric field is the greatest of TE$_{101}$ mode and weakest of TE$_{102}$ mode, as shown in Fig. 8. This will lead to the resonant point of TE$_{101}$ becoming higher, while that of TE$_{102}$ mode is nearly unchanged.

As illustrate in Fig. 8, when the disturbing metallic via-holes are placed at the central axis of resonance cavity R_2, the electric field of TE$_{101}$ mode is compressed greatly, while that of TE$_{102}$ mode
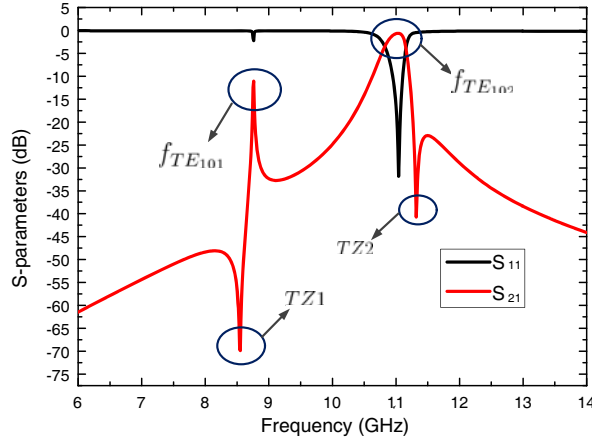
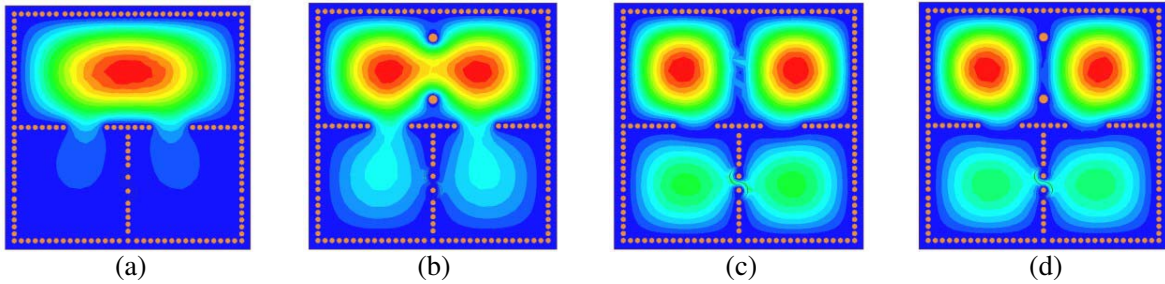**Figure 7.** Simulated S-parameters of the filter shown in Fig. 4.

Figure 8. Electric field distribution in the cavity: (a) TE_{101} mode without disturbing via-holes; (b) TE_{101} mode with disturbing via-holes; (c) TE_{102} mode without disturbing via-holes; (d) TE_{102} mode with disturbing via-holes.

is nearly unaffected.

In the following, we will discuss how to make $f_{TE_{101}}$ come close to $f_{TE_{102}}$ to form a specific passband. The prototype of our filter is shown in Fig. 9.

As shown in Fig. 10(a), we can see that $f_{TE_{101}}$ will be improved with $f_{TE_{102}}$ almost unchanged when the disturbing metallic via-holes come to each other, i.e., S_3 increases. We can also observe that $f_{TE_{101}}$ will shift obviously when the diameter of the via-holes, i.e., D_4, changes. In other words, $f_{TE_{101}}$ is improved with increasing D_4, while $f_{TE_{102}}$ is nearly unaffected, as shown in Fig. 10(b). This is because the electric field of TE_{102} mode is null along the central axis in cavity R_2.

Next, we present an optimized design scheme of the proposed filter. The S-parameters is shown in Fig. 11.

It can be observed that the center frequency of the filter is 11.01 GHz, and the 3 dB FBW is 3.6% running from 10.81 GHz to 11.21 GHz. The insertion loss is lower than 0.6 dB, and the return loss is less than -26 dB. The two TZs are at 10.69 GHz and 11.32 GHz, respectively. The 20 dB rectangular coefficient of the filter is 1.4.

Table 2. Phase of the CT with dual-mode resonance cavity shown in Fig. 4.

path	Below resonance	Above resonance
R_1-R_2-R_3	$-90° - 90° - 90° = -270°$	$-90° + 90° - 90° = -90°$
R_1-R_3	$+90°$	$+90°$
Result	in phase	out of phase
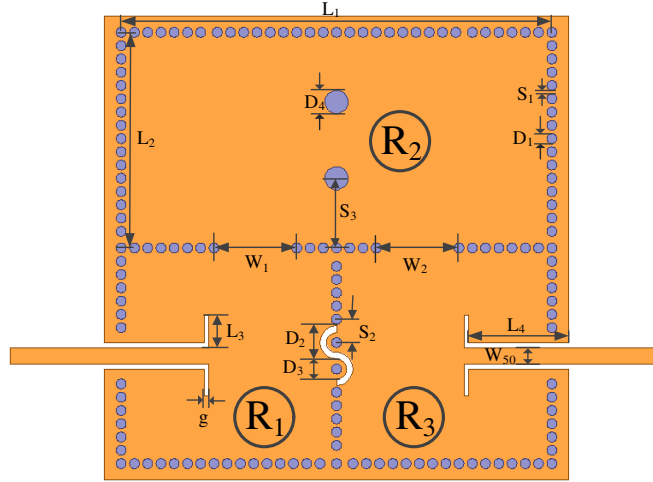
Figure 9. Top view of the proposed filter.
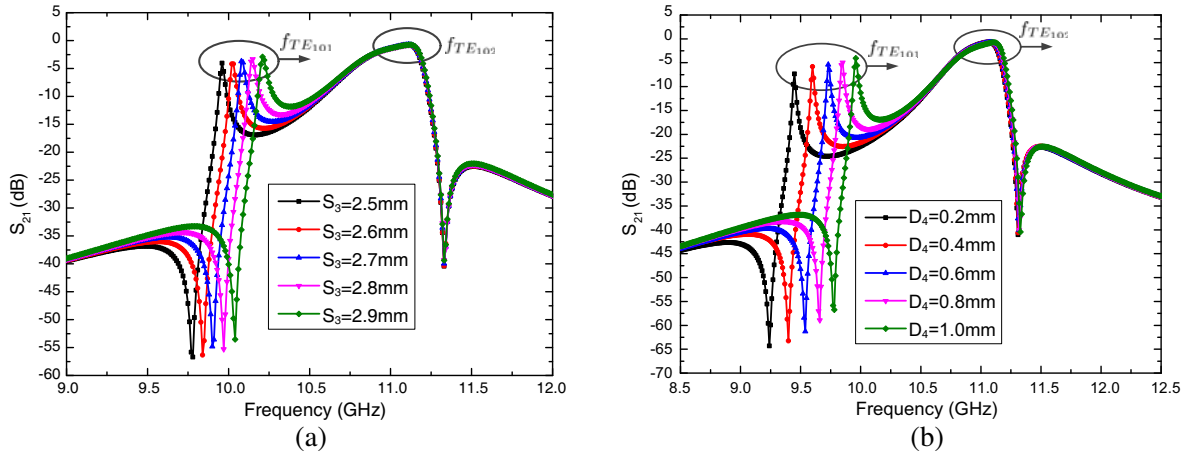
Figure 10. (a) The effect of S_3 to $f_{\mathrm{TE}_{101}}$ and $f_{\mathrm{TE}_{102}}$ with $D_4 = 1.0\,\mathrm{mm}$, (b) the effect of D_4 to $f_{\mathrm{TE}_{101}}$ and $f_{\mathrm{TE}_{102}}$ with $S_3 = 2.5\,\mathrm{mm}$.

The phase model can be summarized in Fig. 12. The left TZ is produced by the phase difference between the path R_1-R_3 and the path R_1-R_2 (TE$_{101}$ mode)-R_3, while the right one arises by the phase difference between the path R_1-R_3 and the path R_1-R_2 (TE$_{102}$ mode)-R_3.

2.4. Controllable Bandwidth

Since the resonant frequency of TE$_{101}$ mode, i.e., $f_{\mathrm{TE}_{101}}$, mainly depends on the size and the position of the disturbing via-holes. It is helpful to design a filter with desirable performance, such as the bandwidth. To this end, we can adjust the dimensions of S_3 and D_4. The simulated results are shown in Fig. 13. With the increase of S_3, the bandwidth of the filter becomes narrow without changing the upper band. When D_4 increases, both the lower band and upper band will move to higher frequencies; however, improvement of the former is much larger than the latter, which also results in a narrower bandwidth.

3. RESULT AND DISCUSSION

To testify the proposed scheme, a filter sample has been fabricated, as demonstrated in Fig. 14. The thickness of the substrate is $0.508\,\mathrm{mm}$, and the relative dielectric constant is 2.2. The dimension of
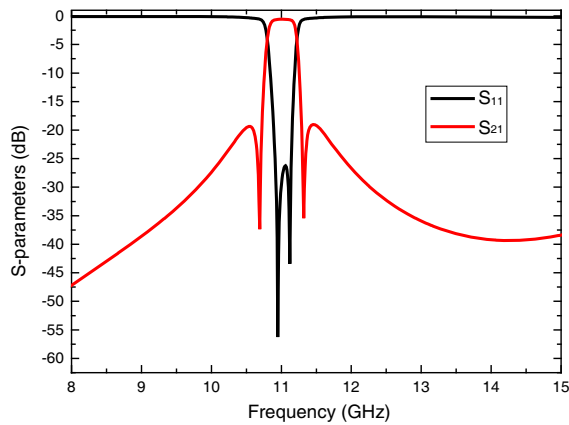
Figure 11. Simulated S-parameters of the proposed filter with dimensions: $W_1 = 5$, $W_2 = 5$, $L_1 = 26$, $L_2 = 13$, $L_3 = 1.92$, $L_4 = 5.5$, $S_1 = 0.8$, $S_2 = 1.4$, $S_3 = 4.3$, $g = 0.3$, $W_{50} = 1$, $D_1 = 0.3$, $D_2 = 2$, $D_3 = 1.2$, $D_4 = 1.0$ (all in mm).
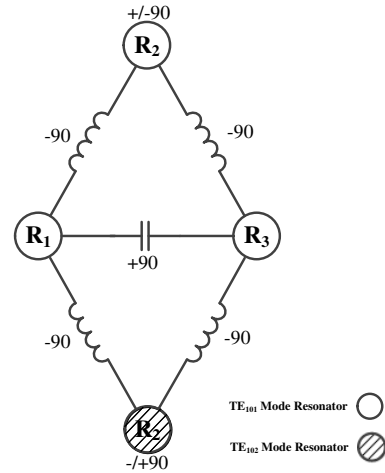

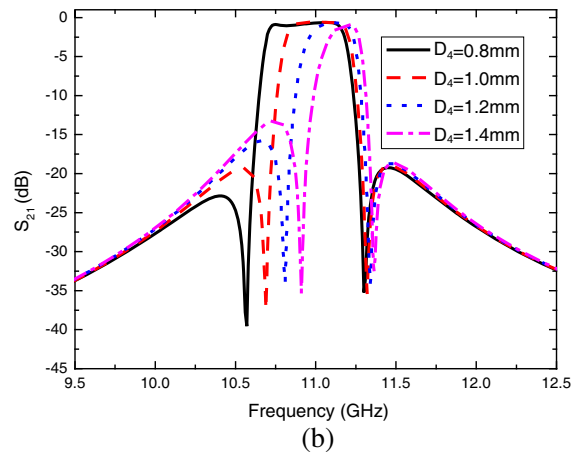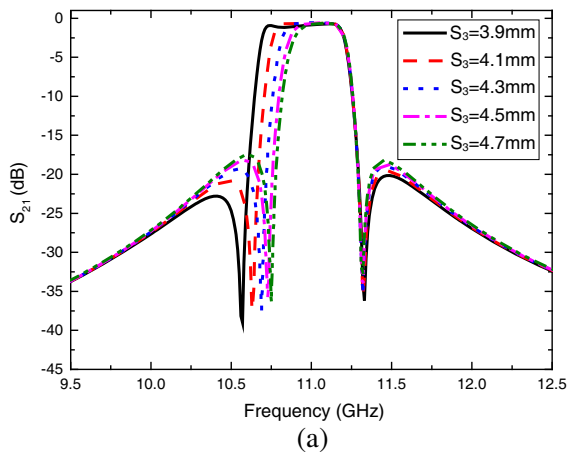**Figure 12.** Phase model of the proposed filter.

Figure 13. Variation of the bandwidth by adjusting the via-holes. (a) S_3 with $D_4 = 1.0$ mm, (b) D_4 with $S_3 = 4.3$ mm.

Figure 14. Photograph of the proposed filter. (a) Top view, (b) layer view.
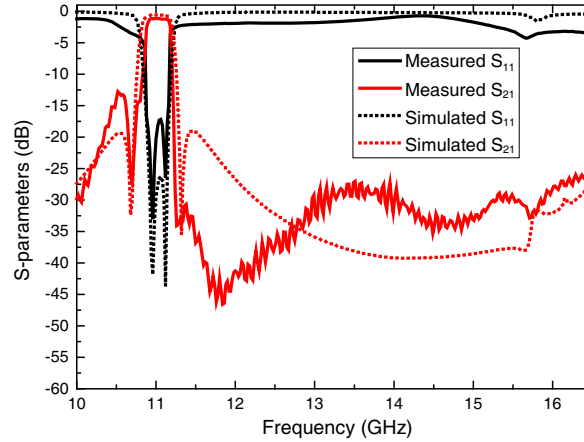
Figure 15. Simulated and measured S-parameters of the proposed filter.

the filter is $1.42\lambda_g \times 1.42\lambda_g$ (excluding the feedlines), where λ_g denotes the dielectric wavelength at the frequency of 11.03 GHz. The measured and simulated scattering parameters are depicted in Fig. 15. Good agreement is observed. As can be seen, the measured 3 dB bandwidth runs from 10.89 GHz to 11.17 GHz, which leads to a center frequency of 11.03 GHz and 3 dB FBW of 2.5%. Within the whole passband, the measured insertion loss is lower than 1.3 dB, which includes the influence of the SMA connectors. The return loss is less than -15 dB. Two TZs are located at 10.69 GHz and 11.25 GHz.

4. CONCLUSION

In this paper, an SIW quasi-elliptic filter with a controllable bandwidth is proposed by combing the cross coupling with dual-mode resonance cavity theory. Owing to the traditional CT structure and the disturbing metallic via-holes in the dual-mode cavity, the SIW cavities can form a desirable passband and two TZs. As a result, the filter has a sharp stopband rejection level, high frequency-selectivity, low insertion loss and wide stopband. A sample has been fabricated and measured. The measured results are in good agreement with the simulated ones.

REFERENCES

1. Deslandes, D. and K. Wu, "Integrated microstrip and rectangular waveguide in planar form," *IEEE Microwave & Wireless Components Letters*, Vol. 11, No. 2, 68–70, 2002.

2. Chen, X. P. and K. Wu, "Self-packaged millimeter-wave substrate integrated waveguide filter with asymmetric frequency response," *IEEE Transactions on Components Packaging & Manufacturing Technology*, Vol. 2, No. 5, 775–782, 2012.

3. Gong, K., W. Hong, Y. Zhang, P. Chen, and C. J. You, "Substrate integrated waveguide quasi-elliptic filters with controllable electric and magnetic mixed coupling," *IEEE Transactions on Microwave Theory & Techniques*, Vol. 60, No. 10, 3071–3078, 2012.

4. You, C. J., Z. N. Chen, X. W. Zhu, and K. Gong, "Single-layered SIW post-loaded electric coupling-enhanced structure and its filter applications," *IEEE Transactions on Microwave Theory & Techniques*, Vol. 61, No. 1, 125–130, 2013.

5. Zhang, D., P. Zhou, Z. Yu, and J. Zhou, "Ka-band quadruple SIW filter with controllable transmission zeros," *IEEE International Conference on Microwave and Millimeter Wave Technology*, 296–298, 2016.

6. Liu, Z., G. Xiao, and L. Zhu, "Triple-mode bandpass filters on CSRR-loaded substrate integrated waveguide cavities," *IEEE Transactions on Components, Packaging and Manufacturing Technology*, Vol. 6, No. 7, 1099–1105, 2016.

7. Rezaee, M. and A. R. Attari, "Realisation of new single-layer triple-mode substrateintegrated waveguide and dual-mode half-mode substrate-integrated waveguide filters using a circular shape perturbation," *IET Microwaves Antennas & Propagation*, Vol. 7, No. 14, 1120–1127, 2013.

8. Zhu, X. C., et al., "Design and implementation of a triple-mode planar filter," *IEEE Microwave & Wireless Components Letters*, Vol. 23, No. 5, 243–245, 2013.

9. Thomas, J. B., "Cross-coupling in coaxial cavity filters — A tutorial overview," *IEEE Transactions on Microwave Theory & Techniques*, Vol. 51, No. 4, 1368–1376, 2003.

10. Wong, S. W., R. S. Chen, J. Y. Lin, L. Zhu, and Q. X. Chu, "Substrate integrated waveguide quasi-elliptic filter using slot-coupled and microstrip-line cross-coupled structures," *IEEE Transactions on Components, Packaging and Manufacturing Technology*, Vol. 6, No. 12, 1881–1888, 2016.

11. Chen, X. P. and K. Wu, "Substrate integrated waveguide cross-coupled filter with negative coupling structure," *IEEE Transactions on Microwave Theory and Techniques*, Vol. 56, No. 1, 142–149, Jan. 2008.

12. Li, M., C. Chen, and W. Chen, "Miniaturized dual-band filter using dual-capacitively loaded SIW cavities," *IEEE Microwave & Wireless Components Letters*, Vol. 27, No. 4, 344–346, 2017.